Controllable Dispersion of Domain-Wall Movement in Antiferromagnetic Thin Films at Finite Temperatures

Yuriy G. Semenov,[1] Xinyi Xu,[1] and Ki Wook Kim[1,2,*]

[1] *Department of Electrical and Computer Engineering, North Carolina State University, Raleigh, North Carolina 27695, USA*

[2] *Department of Physics, North Carolina State University, Raleigh, North Carolina 27695, USA*

(Received 13 February 2019; revised manuscript received 20 May 2019; published 21 June 2019)

The dynamics of a 90° domain wall in an antiferromagnetic nanostrip driven by the current-induced spin-orbit torque are theoretically examined in the presence of thermal fluctuations. A soliton-type equation of motion is developed on the basis of energy balance between the driving forces and dissipative processes in terms of the domain-wall velocity. Comparison with micromagnetic simulations in the deterministic conditions shows good agreement in both the transient and steady-state transport. When the effects of thermal fluctuations are included via a stochastic treatment, the results clearly indicate that the dispersion in the domain-wall position can be controlled electrically by tailoring the strength and duration of the driving current mediating the spin orbital torque in the antiferromagnet. More specifically, the standard deviation of the probability distribution function for the domain-wall movement can be tuned widely while maintaining the average position unaffected. Potential applications of this unusual functionality include probabilistic computing such as Bayesian learning.

DOI: 10.1103/PhysRevApplied.11.064051

I. INTRODUCTION

Effective control of domain walls (DWs) in antiferromagnetic (AFM) materials remains a vital challenge for prospective spintronic applications [1,2]. Despite the challenge, they also offer key advantages over their ferromagnetic counterparts. For instance, there are numerous antiferromagnets with very stiff DWs due to the strong internal exchange interaction, leading to a low effective mass of the DW and no Walker breakdown. Accordingly, the AFM DW device is expected to provide a much faster speed of operation and the corresponding advantages in the driving current (requiring much less energy) [1,2]. A number of approaches explored thus far have demonstrated the desired control. For instance, the effect of the spin-transfer torque was able to manipulate AFM DWs [3–5]. Similarly, the AFM DW transfer can be induced as a result of spin-wave-mediated forces [6,7], which are enhanced by the Dzyaloshinskii-Moriya interaction [8]. In fact, the Dzyaloshinskii-Moriya interaction also assists the DW movement in the presence of a rotating magnetic field [9]. Further, the normally ineffective magnetic field was shown to control the AFM DW velocity when its spatial gradient is combined with a charge current or more precisely, the spin-transfer effect [10,11]. However, the most accessible mechanism for the control of DW dynamics in AFM thin films appears to be the spin-orbit torque (SOT). The electric current through a noncentrosymmetric antiferromagnet generates a SOT associated with a staggered (or Néel-order) field [12–14]. More specifically, a relativistic fieldlike torque can originate from the current-induced local spin polarization with alternating sign between the two sublattices and can couple effectively to the Néel order. Nevertheless, the relevant examples can be found only in a limited class of materials with strong spin-orbit coupling and broken inversion symmetry (e.g., (Cu,Mn)As). An alternative, possibly more widely applicable approach is to exploit the antidamping SOT induced at the interface with a strongly spin-orbit-coupled material such as a heavy metal [15].

Specific physical details aside, all of the aforementioned studies have considered the deterministic dynamics essentially in the limit of zero temperature. Furthermore, most of them have focused on the AFM textures in the form of 180° DWs, posing an additional challenge in discriminating the domains with antiparallel Néel vectors. For instance, electrical detection of 180° DW switching or movement is outside the practical realm at the moment as the correspondent magnetoresistance is extremely small (see Ref. [2] for additional details). A more promising alternative may be to utilize the 90° DWs in light of the recent experimental advances in their manipulation and detection [13]. In fact, 90° rotation of the Néel-vector orientation has already been identified in the electrical measurements with a large signal in the anisotropic magnetoresistance [13,14] or its tunneling variety [16]. Furthermore, the induced rotation

*kwk@ncsu.edu

was shown to result in 90° DWs [14]. On the other hand, the theoretical understanding on the dynamics of 90° DWs in the antiferromagnets has received only limited attention [12]. Since the operation is predominantly at ambient conditions, the effect of finite temperature and the subsequent stochastic nature of the DW dynamics also add interesting perspectives.

The uncertainty in the final DW position is evidently undesirable for memory or Boolean-logic applications. On the other hand, controllable stochasticity of the output signals with a desired distribution function has begun to draw much attention since its prospective utilization in machine learning or Bayesian computing. Physical implementation of the concept of probabilistic computing has so far relied predominantly on the external generators of random numbers. While the alternative approaches have also been explored, they tend to involve complex hardware arrangements (see, for instance, Ref. [17] and the references therein). It is clearly desirable if a single device or structure can meet the needs with simple electrical control. The probabilistic effect of the AFM DW motion may offer this unique functionality.

In the present work, we theoretically analyze the 90° DW motion in an AFM thin film driven by the SOT pulse at finite temperatures. A soliton-type treatment is developed from the Lagrangian representation to examine the DW dynamics, including the effect of thermal fluctuations. The results clearly illustrate the characteristics of the AFM DW motion. When subjected to a SOT pulse, the DW undergoes acceleration and then velocity saturation as the dissipation compensates the antidamping torque. Once the driving force is turned off, the inertial phase follows much like an actual particle with nonzero mass. The thermal fields introduce substantial deviations in the DW trajectories depending on the strength and the duration of the driving SOT pulse. The corresponding variation in the probability distribution of the DW position indicates a broad range that can be tuned electrically.

II. THEORETICAL FORMULATION

The structure under consideration is shown in Fig. 1(a). It is essentially a bilayer structure of an AFM nanostrip and a strongly spin-orbit-coupled material that can benefit from the current-induced SOT mentioned earlier [15]. A vertical tunnel junction can be added on top for electrical measurement of the DW position via the tunneling anisotropic magnetoresistance. As the x-directional current flow induces the effective field along the z axis in the present setup, the magnetic domains need to be oriented normal to this axis (z) for efficiency. Accordingly, an antiferromagnet with biaxial anisotropy in the x-y easy plane (such as those with tetragonal D_{4h} symmetry) is assumed for the desired 90° DW. The metallic materials are expected to offer a convenient choice for experimental

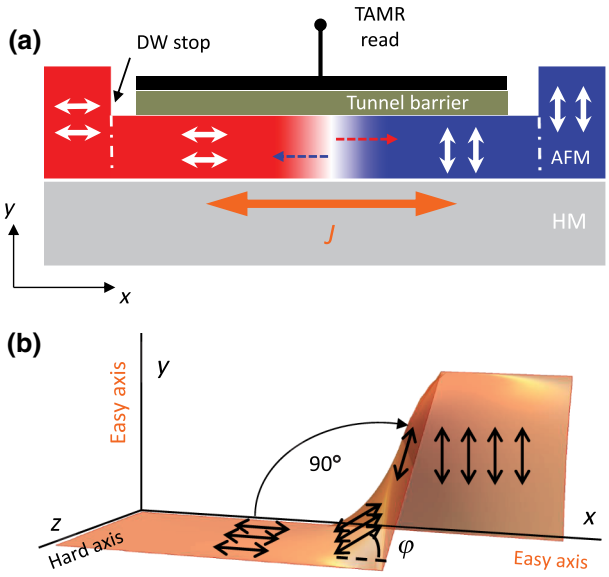

FIG. 1. (a) Schematic illustration of the antiferromagnet-based DW device under consideration. The electric current J through the heavy metal (HM) layer generates the spin current, providing the SOT to the AFM strip necessary for the DW motion. The 90° DW can travel in either direction ($\pm x$) that is determined by the current flow in the HM layer. The shift in the DW position can be detected through the top contact either via the anisotropic magnetoresistance or its tunneling variety (TAMR) as shown. (b) Spin textures of the 90° Néel DW with the heavy z axis and the easy x and y axes.

realization and detection, while similar physical principles can be applied to the dielectric systems as well.

In the analysis, the relatively small cross section of the AFM strip makes it possible to ignore the Néel-vector variation in the y-z plane, reducing the problem to the dynamics in the 1+1 space-time (x, t) coordinates with no additional variables. Thus, the sigma-model equations developed earlier in the literature can be applied to describe the Néel-vector dynamics [18,19]. Since this approach predicts the Néel-vector reorientation only in the x-y plane (provided that the SOT is applied along the hard z axis), the calculation can take advantage of the Lagrangian representation $\mathcal{L}$ in terms of the azimuthal angle $\varphi(x, t)$ between the two easy axes (using x as the reference). A similar formalism developed earlier for an easy-plane antiferromagnet [20] can be directly generalized to the case of biaxial anisotropy with the following term for the anisotropy energy:

$$W_{\text{in}} = \frac{K_\perp}{4}(n_x^4 + n_y^4) = \frac{K_\perp}{4}\left(1 - \frac{1}{2}\sin^2 2\varphi\right) \rightarrow -\frac{K_\perp}{8}\sin^2 2\varphi. \quad (1)$$

Here, $K_\perp$ (< 0) is the biaxial anisotropy constant in the easy x-y plane and $n_{x(y)} = L_{x(y)}/|\mathbf{L}| = \cos\varphi$ ($\sin\varphi$) is the

normalized representation **n** of the Néel vector **L**. The constant term can be neglected without the loss of generality. Similarly, the contribution of the z-directional anisotropy $K_{\parallel}$ (>0) is not considered since n_z does not appear in the dynamical equations. Then, the dimensionless Lagrangian $\mathscr{L} = \mathcal{L}/|K_{\perp}|$ can be reduced to the canonical form in terms of dimensionless time t $(=\omega_r t)$ and space x $(=\omega_r x/v_m)$, i.e.,

$$\mathscr{L} = \frac{1}{2}\dot{\varphi}_t^2 - \frac{1}{2}\dot{\varphi}_x^2 - \frac{1}{8}\sin^2 2\varphi, \tag{2}$$

where $\dot{\varphi}_i \equiv (\partial/\partial i)\varphi$ $(i = x, t)$, $\omega_r = \gamma\sqrt{2H_{\rm ex}H_{\rm an}}$ denotes the zero-field AFM resonance frequency, γ the gyromagnetic ratio, $H_{\rm an} = |K_{\perp}|/\frac{1}{2}L$ the anisotropy field, $H_{\rm ex}$ the exchange field between the magnetic sublattices, and v_m the magnon velocity.

The corresponding Euler-Lagrange equation for an open system subjected to the external forces (i.e., torques) $\rho = \rho(x,t)$ reads

$$\ddot{\varphi}_{tt} - \ddot{\varphi}_{xx} + \frac{1}{4}\sin 4\varphi = \rho. \tag{3}$$

The expression reproduces the sine-Gordon equation in terms of variable 4φ for a conserving system (i.e., when $\rho = 0$) [18]. In this case, the basic solution of Eq. (3) can be written in the form of a soliton moving with velocity v,

$$\varphi = \pm\arctan\left[\exp\left(\frac{x - vt}{\sqrt{1-v^2}}\right)\right]. \tag{4}$$

The effective width $\delta_{\rm DW}$ of the soliton (or the DW) can be estimated as $\pi\sqrt{1-v^2}$. The $\pm$ signs correspond to the $\pm y$ alignment of the Néel vector, respectively, at $x \to \infty$ (i.e., far away from the soliton). As these two directions are equivalent in the present analysis, the $+$ case is chosen for convenience. The corresponding Néel-vector texture $\mathbf{n} = (\cos\varphi, \sin\varphi, 0)$ is shown in Fig. 1(b). Note that the velocity v is also normalized to v_m following the definitions of x and t (thus, $|v| < 1$).

Similarly to Ref. [15], the soliton representation [Eq. (4)] of the DW texture is treated as an ansatz for the analysis of a nonconserving system with energy dissipation and external forces. In such an approximation, only the DW velocity $v = v(x,t)$ remains the actual parameter describing the DW dynamics. To proceed further, the specific form for ρ is needed in Eq. (3). The relevant contributions in the present analysis come from three terms—the energy dissipation via damping, the antidamping SOT from the driving current, and the fieldlike torque from the thermal fluctuations. The resulting expression for $\rho(x,t)$ is given in dimensionless units as [20]

$$\rho = -2\lambda\dot{\varphi}_t + \Phi(x,t) - \frac{\partial h_{\rm th}}{\partial t}, \tag{5}$$

where λ $(=\delta_r/\omega_r)$ is the damping parameter related to the width δ_r of the AFM resonance and $h_{\rm th}$ $(=\gamma H_{\rm th}/\omega_r)$ is the normalized thermal field $H_{\rm th}$. In addition, the second term representing the antidamping SOT of $\eta(\mathbf{n}\times\hat{\mathbf{z}})\cdot\dot{\mathbf{n}}_t$ can be written more explicitly as

$$\Phi(x,t) = \frac{\eta}{M_L^2}\frac{H_{\rm ex}}{2H_{\rm an}}, \tag{6}$$

where M_L denotes the sublattice magnetization $(\simeq \frac{1}{2}L)$. The parameter η reflects the strength of the spin Hall current flowing into the AFM layer [15], through which a potential dependence on position x and time t can be introduced. The reversal of the driving current direction [J in Fig. 1(a)] flips the polarization of the spin Hall current and thus the sign $(\pm)$ of the resulting torque Φ (accounting for the back and forth movement). As stated earlier, $H_{\rm th}$ is a natural source of randomness in the DW trajectories and the dispersion in its final location. With corresponding modifications to Eq. (5), the formalism discussed above can also be applied to the DW transfer driven by the Néel SOT in the asymmetric antiferromagnets [12].

The dynamics of the Néel-vector textures are first examined in the absence of thermal fluctuations, where the current induced SOT unambiguously determines the DW motion. Applying the ansatz of Eq. (4) sufficiently simplifies the problem to the balance of energy flows to and from the DW, avoiding the need to solve Eqs. (3) and (5) directly. In this context, the net mechanical energy of the DW with the Lagrangian given in Eq. (2) becomes

$$E(v) = \int\left(\frac{1}{2}\dot{\varphi}_t^2 + \frac{1}{2}\dot{\varphi}_x^2 + \frac{1}{8}\sin^2 2\varphi\right)dx. \tag{7}$$

The range of integration can be safely set for the entire x axis provided that the structure is much longer than the DW width. Then, for a single 90° wall of Eq. (4), the calculation yields

$$E(v) = \frac{1}{2\sqrt{1-v^2}}, \tag{8}$$

which corresponds to the 1/16 of the energy for the 360° kink described by the sine-Gordon equation. The description in conventional energy units can be restored by multiplying Eq. (8) by the factor AKv_m/ω_r and replacing v with v/v_m. Here, A denotes the cross section of the AFM thin film. Along with Eq. (8), the rate of net energy change (dE/dt) can also be obtained from Eq. (5) as $\int[\Phi - 2\lambda\dot{\varphi}_t]\dot{\varphi}_t dx$. After some algebra, the balance of

energy flow to and from the AFM layer can be written finally in terms of an equation for the DW velocity

$$\frac{1}{2\lambda}\frac{dv}{dt} = \left(-v + Q\sqrt{1-v^2}\right)(1-v^2), \tag{9}$$

where $Q = (\pi/2\lambda)\Phi$. The solution of this expression provides the trajectory of the DW in the deterministic transport (i.e., no thermal fluctuations).

The equation of motion for the DW can be solved analytically under simple conditions. Assuming the initial stationary state $x = 0$ at $t = 0$ and a constant SOT Q applied for a duration t_p, Eq. (9) yields

$$v_Q(t) = \frac{Q(1-e^{-2\lambda t})}{\sqrt{Q^2(1-e^{-2\lambda t})^2 + 1}}, \quad 0 < t \leq t_p. \tag{10}$$

The DW velocity increases linearly as $v_Q(t) = 2\lambda Qt = \pi\Phi t$ in the beginning stage and then shows a saturation pattern once the dissipation compensates the antidamping SOT as $t \gg 1/2\lambda$ (see also Ref. [18]),

$$v_s = \frac{Q}{\sqrt{Q^2+1}}. \tag{11}$$

This steady-state velocity v_s reaches the maximal magnon velocity v_m (= 1) in the limit of $\lambda \to 0$ or $Q \to \infty$. Another interesting observation from Eq. (9) is that the velocity does not drop to zero even after the driving force is turned off. With the initial velocity of v_p at $t = t_p$ [i.e., $v_p = v_Q(t_p)$], the solution illustrates the characteristic inertial motion with

$$v_0(t) = \frac{v_p}{\sqrt{e^{4\lambda(t-t_p)}(1-v_p^2) + v_p^2}}, \quad t > t_p. \tag{12}$$

The dynamics overall appear much like those of actual particles with nonzero mass. In contrast, the DWs in a ferromagnet would stop moving as soon as the external torque ceases. Note that the velocity can take the negative sign following the parameter Q (thus, the antidamping SOT Φ). This simply indicates that the DW is moving in the $-x$ direction as briefly discussed earlier. In the current analysis, we implicitly assume the driving conditions that result in the transport along the $+x$ direction using $x = 0$ as the reference (i.e., positive Q).

The AFM DW trajectory in the real space can be subsequently calculated by integrating the velocity over time. When the time of interest is longer than the pulse duration, the distance of travel includes the contribution by the inertia given by

$$x_p(t) = \frac{1}{4\lambda}\ln\left[\frac{1+v_p}{1-v_p}\times\frac{1-v_0(t)}{1+v_0(t)}\right], \quad t > t_p. \tag{13}$$

Interestingly, this expression also characterizes the length that a DW moving with the velocity v_p would travel unpropelled before losing all of the energy and coming to a stop (i.e., via inertia):

$$x_p(t\to\infty) \quad \Rightarrow \quad x_{\rm in}(v_p) = \frac{1}{4\lambda}\ln\frac{1+v_p}{1-v_p}. \tag{14}$$

Another factor that must be considered in the DW movement is the effect of the coercivity. In the real structures, the defects like the grain boundaries and impurities may pin the DW. They keep the DW from slipping via the Brownian thermal motion. Otherwise, the diffusive dispersion in the DW position would diverge as time t goes to infinity [21]. The present formalism can readily account for the nonzero coercivity by introducing a lower bound to the kinetic energy for displacement. In this picture, the DW gets pinned as soon as the kinetic energy $[E(v) - E(0)$; see Eq. (8)] becomes smaller than the trapping energy $H_c M_L A \delta_{\rm DW}$, where H_c denotes the effective field for coercivity. The impact of finite coercivity is particularly relevant during the inertial phase of the DW transport where the unpropelled movement is susceptible to the external factors. While the DW is being driven ($t \leq t_p$) on the other hand, we may not need an additional consideration so long as the applied SOT is sufficiently strong. A corresponding criterion can be expressed in terms of the critical velocity $v_c = \sqrt{4\pi H_c M_L/|K_\perp|}$ provided $v_c \ll 1$. Since H_c cannot be determined *a priori* in terms of the material parameters, v_c is treated as an independent phenomenological constant for the coercivity of a particular structure.

The expressions given above provide a complete solution to the problem of the DW dynamics driven by an electric current pulse. Under the pulse duration t_p with amplitude Q, the net displacement becomes

$$x_0 = x_Q(t_p) + x_{\rm in}(v_p) - x_{\rm in}(v_c), \tag{15}$$

where $x_Q(t_p)$ $[= \int_0^{t_p} v_Q(t)dt]$ denotes the distance traveled while being driven and $x_{\rm in}(v_c)$ accounts for the reduction in the free flight (i.e., the inertial transport) due to the coercivity. Conversely, they can also be solved to deduce the relationship between t_p and Q for the desired x_0. It is evident that a shorter pulse duration is sufficient when the SOT amplitude is stronger and vice versa.

III. RESULTS AND DISCUSSION

A. Model validation

Before proceeding further, it is necessary to examine the validity of the adopted treatment based on the soliton description [Eq. (4)]. For this, a direct comparison is made with the micromagnetic simulation of the AFM DW dynamics [22]. The calculations are carried out for the AFM slab with the dimensions of $3000 \times 50 \times 20$ nm^3. The numerical parameters adopted from typical AFM materials (e.g., Mn_2Au [23–25]) are the sublattice magnetization $M_L = 780$ G, the anisotropy energies $K_\perp = -2.1 \times 10^5$ erg cm^{-3}, $K_\parallel = 6.6 \times 10^7$ erg cm^{-3}, and the exchange stiffness $A_{ex} = 1.7 \times 10^{-6}$ erg/cm. These correspond to the exchange field $H_{ex} = 1.3 \times 10^7$ G, the anisotropy field $H_{an} = 300$ G, the resonant frequency $\omega_r = 2\pi \times 160$ GHz, and the magnon velocity $v_m = 3 \times 10^6$ cm/s. In addition, the Gilbert damping constant α_G is taken to be 0.001 that yields the damping parameter $\lambda = 0.104$. The relation between the SOT Q and the current density J (i.e., Q/J) is estimated to be 0.114 nm^2/nA with the effective spin Hall angle of 0.1 [15]. The effect of coercivity is not considered for the comparison due to the limitation of the micromagnetic simulation.

The calculations reveal the nonlinear dependence of the DW velocity on the pulse intensity. As shown in Fig. 2(a), the AFM DW when subjected to an SOT pulse undergoes acceleration initially and then velocity saturation with the dissipation compensating the antidamping SOT. Once the driving force is turned off, the inertial phase follows. Using the dimensional units, both the analytical solution and the results of the micromagnetic simulations are plotted in Figs. 2(b) and 2(c). A good agreement is observed between the two approaches in both the steady-state transport and the transient conditions with the inertial motion [Figs. 2(b) and 2(b), respectively], providing credence to the validity of the developed model. With the soliton ansatz verified, Eq. (9) can be expanded to account for the stochastic thermal motions in the DW dynamics at finite temperatures.

B. Effects of thermal fluctuations

The analysis of the thermal field influence on the DW transport supposes evaluation of thermal fluctuations h_{th} along the entire DW path. On the other hand, the perturbations away from the location of the wall texture are unlikely to affect the DW dynamics. The actual range of the AFM channel where the influence of random motions needs to be considered is the relatively narrow stretch corresponding to the wall texture (i.e., the DW width δ_{DW}). Thus the problem can be approximated to the analysis of the fluctuation effect in the finite volume of $V = A \times \delta_{DW}$ associated with the soliton representation. Accordingly, the influence of the thermal field can be accounted for by conveniently adding a randomly fluctuating fieldlike torque [i.e., $-(\pi/2\lambda)(d/dt)h_{th}(t)$] to the current-induced SOT Q in the dynamical equation governing the soliton motion [see also Eq. (5)].

In describing the thermal field $h_{th}(t)$, the approximation based on a series of random step functions used commonly in the ferromagnetic systems cannot be applied here due to the explicit dependence on the time derivative [26]. As an alternative, a spectral representation is adopted in the form of a Fourier series expansion with random amplitudes [27]. This representation allows straightforward introduction of the upper and lower bounds in the noise spectrum by considering the autocorrelation time τ_c and the characteristic Néel-vector relaxation time τ_m (more precisely, the inverses $2\pi/\tau_c$ and $2\pi/\tau_m$, respectively). Furthermore, the fact that the lower truncation frequency $2\pi/\tau_m$ corresponds to the broadening of the AFM resonant frequency

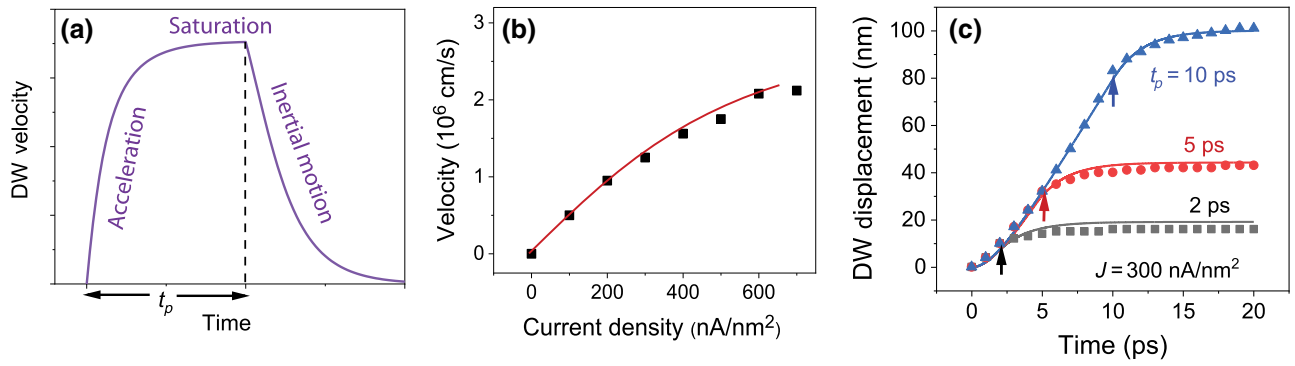

FIG. 2. Comparison of the calculation results with the micromagnetic simulations in the deterministic transport (i.e., without thermal motions). (a) Characteristic evolution of the 90° DW velocity in the thin-film AFM strip under a SOT pulse with duration t_p. (b) Steady-state DW velocity versus the driving current density in the HM layer. (c) DW position as a function of time for different SOT pulse durations. The vertical arrows indicate the instants when the SOT is turned off. The driving current density J is fixed at 300 nA/nm^2. In (b),(c), the data points are from micromagnetic simulations while the solid curves show the results from the model calculations. An excellent agreement is observed between them in both the steady-state and transient transport. The effect of coercivity is not considered here.

δ_r ($= \lambda\omega_r$) offers a physical ground for the discretization of the spectral domain in the comparable intervals. As the response of a damped Néel-vector motion becomes practically invariant to the perturbation frequency swing in the range of δ_r due to the broadening, the actual noise spectrum can be discretized likewise.

In other words, the AFM response to the thermal noise is virtually equivalent to a series of sinusoidal perturbations with random amplitudes and the frequencies $n\delta_r$ ($n = 1, 2, \ldots, N$, where N is given by τ_m/τ_c). The fluctuation dissipation theorem defines the amplitude of fluctuating field in the form [27],

$$h_{\rm th}(t) = \frac{\delta_r}{\omega_r}\left(\frac{2k_BT}{NV|K_\perp|}\right)^{1/2} \times \left(\sum_{n=1}^{N}\alpha_n \sin n\frac{\delta_r}{\omega_r}t + \sum_{n=1}^{N}\beta_n \cos n\frac{\delta_r}{\omega_r}t\right), \quad (16)$$

where k_BT denotes the thermal energy, $n(\delta_r/\omega_r)t$ is actually $n\delta_r t$ in physical units, and $1/2N\sum_{n=1}^{N}\langle\alpha_n^2 + \beta_n^2\rangle = 1$. Note that the noise expression applies only for a duration up to τ_m in the time domain due to the relaxation. A time period longer than this interval requires repeated random selections. Equation (16) is clearly differentiable that can be directly incorporated into Eq. (9). The exact details of the noise model including a particular choice of the material parameters are not highly crucial in examining the possible electrical control in the thermally induced dispersion of the DW position.

Before accounting for the thermal component, Fig. 3 first examines the deterministic relation between the necessary SOT pulse strength and the duration for a desired travel distance x_0. The results are plotted in a normalized form in terms of $2\lambda t_p$ and $2\lambda x_0$ since it conveniently circumvents the explicit dependence on other physical parameters [see, for instance, Eqs. (10) and (14)]. The coercivity of $v_c = 0.01$ is considered as well to reflect the conditions in the realistic structures [Eq. (15)]. As shown, both short and strong (red) as well as long and weak (blue) pulses can shift the DW by the same distance. The obtained relation serves as the guideline for the desired mean or average motion of the AFM DWs.

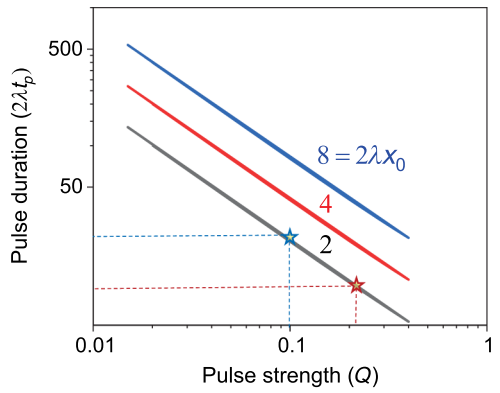

FIG. 3. Calculated SOT pulse strength versus the duration for three travel distances x_0 in the deterministic transport. The results are plotted in normalized units in terms of $2\lambda t_p$ and $2\lambda x_0$ to circumvent the explicit dependence on other physical parameters. The coercivity of $v_c = 0.01$ is also included in the analysis. The blue and red points highlight two different conditions ($Q = 0.1$ and 0.21, respectively) that shift the DW by the same distance.

Once the influence of thermal fluctuations is accounted for, the DW dynamics deviates from the prescribed path [see the inset to Fig. 4(a)]. The resulting dispersion in the final position $x_{\rm DW}$ around x_0 can be calculated by numerically solving Eq. (9) in the presence of the random fieldlike torque $-(\pi/2\lambda)(d/dt)h_{\rm th}(t)$. A sufficiently large number of iterations N_i are needed to ensure a statistically reliable outcome due to the stochastic nature of the calculation. Likewise the magnitude of the autocorrelation time τ_c is treated empirically. Since our analysis is not significantly affected by the exact value of τ_c so long as it is sufficiently shorter than τ_m, a small constant fraction ($\tau_c = 0.01\tau_m$; $N = 100$) is assumed for simplicity in Eq. (16). For a set of given conditions, the calculations are repeated 250 times ($= N_i$), each with an independently selected $h_{\rm th}(t)$ pattern randomly varying in time.

Figure 4(a) shows the typical probability distribution of the DW position for two SOT pulses at 300 K. While both pulses are designed to shift the DW by the same distance on average (see also two points marked in Fig. 3), the dispersion as the result of thermal motion shows a significant difference. The short and strong pulse (red; $Q = 0.21$) produces a much narrower distribution than the long and weak counterpart (blue; $Q = 0.1$). It can be intuitively understood that the DW driven by a strong pulse is less likely to be influenced by the comparatively minor thermal fluctuations. At the same time, the DW is exposed to the random motions for a shorter duration in this case for it reaches the final destination quicker and then pinned by the coercivity. It is also interesting to note that the mean position $\langle x_{\rm DW}\rangle$ averaged over N_i iterations is indeed given by x_0 as designed (from the deterministic analysis), with high accuracy. Since the pulse strength and duration can be controlled electrically, the probability distribution function in the DW position can be tuned likewise (i.e., narrower $\rightleftarrows$ broader). Combined with the structure utilizing the anisotropic magnetoresistance, as shown in Fig. 1(a) [13,16,28], it can be translated into a corresponding probabilistic distribution in the electrical output signal—an essential component in probabilistic computing or Bayesian learning.

Finally, Fig. 4(b) plots the normalized standard deviation in the DW position $\Delta = \left\langle(x_{\rm DW}/\langle x_{\rm DW}\rangle - 1)^2\right\rangle^{1/2}$ as a function of Q for three average displacements at $T =$ 300 K. The calculations of Δ at different temperatures reproduce a similar dependence on Q with a prefactor that

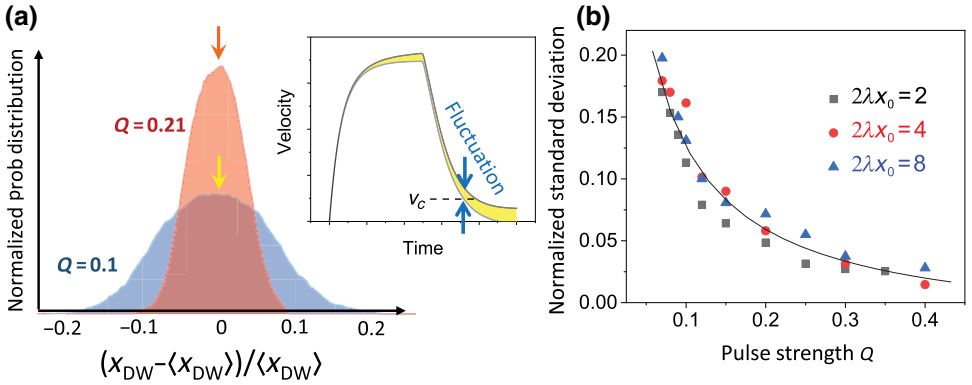

FIG. 4. (a) Probability distribution of the DW position x_{DW} at 300 K calculated for two SOT pulses ($Q = 0.21$ and $Q = 0.1$ corresponding to the red and blue marks in Fig. 3, respectively). The horizontal axis shows the normalized deviation from the average position $\langle x_{DW}\rangle$, which matches with x_0 from the deterministic analysis. The inset schematically illustrates the effect of thermal fluctuations on the DW velocity. (b) Normalized standard deviation in the DW position as a function of the SOT strength for three average displacements x_0. The pulse duration corresponding to each Q and x_0 can be found in Fig. 3. The solid curve represents a fit with an inverse proportionality aQ^{-1} ($a = 0.012$). The coercivity ($v_c = 0.01$) is accounted for in both (a),(b).

is proportional to $\sqrt{T}$. In fact, this $\sqrt{T}$ scaling is consistent with that anticipated from the fluctuation dissipation theorem [i.e., the temperature dependence of the fluctuating field amplitude; see Eq. (16)]. The observed large differences in Δ indicate that a broad range of probability distributions can be realized with a single AFM device. Moreover, the normalized deviation appears to be only weakly dependent on x_0 or $\langle x_{DW}\rangle$ (thus, on the pulse duration t_p for a given Q). Clearly, the determining factor is the pulse strength Q, to which Δ exhibits an inverse proportionality.

IV. SUMMARY

The fluctuating thermal fields in the antiferromagnets are identified as a potential mechanism to realize a probabilistic distribution in the electrical output signal, whose characteristic properties such as the standard deviation may also be tailored conveniently by electrical control. To this end, the dynamics of a 90° DW driven by the current-induced SOT is theoretically examined at finite temperatures in a thin-film AFM structure. A soliton-type representation based on an energy balance equation is developed to describe the DW motion in combination with a stochastic thermal field model for AFM nanoparticles. The calculation results clearly illustrate that both the average displacement of the DW position and its thermally induced dispersion can be modulated electrically by simply tuning the driving SOT strength and the duration. The corresponding probabilistic response in the electrical output signal via the magnetoresistance offers an effective means to realize the probability distribution functions that can be "trained." This unusual functionality may provide a key component in the emerging probabilistic computing and machine-learning architectures.

ACKNOWLEDGMENT

This work is supported, in part, by the US Army Research Office (W911NF-16-1-0472).

[1] O. Gomonay, T. Jungwirth, and J. Sinova, Concepts of antiferromagnetic spintronics, Phys. Status Solidi RRL **11**, 1700022 (2017).
[2] V. Baltz, A. Manchon, M. Tsoi, T. Moriyama, T. Ono, and Y. Tserkovnyak, Antiferromagnetic spintronics, Rev. Mod. Phys. **90**, 015005 (2018).
[3] K. M. D. Hals, Y. Tserkovnyak, and A. Brataas, Phenomenology of Current-induced Dynamics in Antiferromagnets, Phys. Rev. Lett. **106**, 107206 (2011).
[4] A. C. Swaving and R. A. Duine, Current-induced torques in continuous antiferromagnetic textures, Phys. Rev. B **83**, 054428 (2011).
[5] E. G. Tveten, A. Qaiumzadeh, O. A. Tretiakov, and A. Brataas, Staggered Dynamics in Antiferromagnets by Collective Coordinates, Phys. Rev. Lett. **110**, 127208 (2013).
[6] S. K. Kim, Y. Tserkovnyak, and O. Tchernyshyov, Propulsion of a domain wall in an antiferromagnet by magnons, Phys. Rev. B **90**, 104406 (2014).
[7] E. G. Tveten, A. Qaiumzadeh, and A. Brataas, Antiferromagnetic Domain Wall Motion Induced by Spin Waves, Phys. Rev. Lett. **112**, 147204 (2014).
[8] A. Qaiumzadeh, L. A. Kristiansen, and A. Brataas, Controlling chiral domain walls in antiferromagnets using spin-wave helicity, Phys. Rev. B **97**, 020402(R) (2018).
[9] K. Pan, L. Xing, H. Y. Yuan, and W. Wang, Driving chiral domain walls in antiferromagnets using rotating magnetic fields, Phys. Rev. B **97**, 184418 (2018).
[10] D. R. Rodrigues, K. Everschor-Sitte, O. A. Tretiakov, J. Sinova, and Ar. Abanov, Spin texture motion in antiferromagnetic and ferromagnetic nanowires, Phys. Rev. B **95**, 174408 (2017).

[11] Y. Yamane, O. Gomonay, H. Velkov, and J. Sinova, Combined effect of magnetic field and charge current on antiferromagnetic domain-wall dynamics, Phys. Rev. B **96**, 064408 (2017).

[12] O. Gomonay, T. Jungwirth, and J. Sinova, High Antiferromagnetic Domain Wall Velocity Induced by Néel Spin-orbit Torques, Phys. Rev. Lett. **117**, 017202 (2016).

[13] S. Yu. Bodnar, L. Šmejkal, I. Turek, T. Jungwirth, O. Gomonay, J. Sinova, A. A. Sapozhnik, H.-J. Elmers, M. Kläui, and M. Jourdan, Writing and reading antiferromagnetic Mn_2Au by Néel spin-orbit torques and large anisotropic magnetoresistance, Nat. Commun. **9**, 348 (2018).

[14] P. Wadley, S. Reimers, M. J. Grzybowski, C. Andrews, M. Wang, J. S. Chauhan, B. L. Gallagher, R. P. Campion, K. W. Edmonds, S. S. Dhesi, F. Maccherozzi, V. Novak, J. Wunderlich, and T. Jungwirth, Current polarity-dependent manipulation of antiferromagnetic domains, Nat. Nanotechnol. **13**, 362 (2018).

[15] T. Shiino, S.-H. Oh, P. M. Haney, S.-W. Lee, G. Go, B.-G. Park, and K.-J. Lee, Antiferromagnetic Domain Wall Motion Driven by Spin-orbit Torques, Phys. Rev. Lett. **117**, 087203 (2016).

[16] B. G. Park, J. Wunderlich, X. Martí, V. Holý, Y. Kurosaki, M. Yamada, H. Yamamoto, A. Nishide, J. Hayakawa, H. Takahashi, A. B. Shick, and T. Jungwirth, A spin-valve-like magnetoresistance of an antiferromagnet-based tunnel junction, Nat. Mater. **10**, 347 (2011).

[17] D. Pinna, F. Abreu Araujo, J.-V. Kim, V. Cros, D. Querlioz, P. Bessiere, J. Droulez, and J. Grollier, Skyrmion Gas Manipulation for Probabilistic Computing, Phys. Rev. Appl. **9**, 064018 (2018).

[18] V. G. Bar'yakhtar, B. A. Ivanov, and M. V. Chetkin, Dynamics of domain walls in weak ferromagnets, Sov. Phys. Uspekhi **28**, 563 (1985).

[19] B. A. Ivanov, Mesoscopic antiferromagnets: Statics, dynamics, and quantum tunneling (review), Low Temp. Phys. **31**, 635 (2005).

[20] Y. G. Semenov, X.-L. Li, X. Xu, and K. W. Kim, Helical waves in easy-plane antiferromagnets, Phys. Rev. B **96**, 224432 (2017).

[21] Z. Yan, Z. Chen, M. Qin, X. Lu, X. Gao, and J. Liu, Brownian motion and entropic torque driven motion of domain walls in antiferromagnets, Phys. Rev. B **97**, 054308 (2018).

[22] X. Li, X. Duan, Y. G. Semenov, and K. W. Kim, Electrical switching of antiferromagnets via strongly spin-orbit coupled materials, J. Appl. Phys. **121**, 023907 (2017).

[23] V. M. T. S. Barthem, C. V. Colin, H. Mayaffre, M.-H. Julien, and D. Givord, Revealing the properties of Mn_2Au for antiferromagnetic spintronics, Nat. Commun. **4**, 2892 (2013).

[24] M. Arana, F. Estrada, D. S. Maior, J. B. S. Mendes, L. E. Fernandez-Outon, W. A. A. Macedo, V. M. T. S. Barthem, D. Givord, A. Azevedo, and S. M. Rezende, Observation of magnons in Mn_2Au films by inelastic Brillouin and Raman light scattering, Appl. Phys. Lett. **111**, 192409 (2017).

[25] M. Mainert, D. Graulich, and T. Matalla-Wagner, Electrical Switching of Antiferromagnetic Mn_2Au and the Role of Thermal Activation, Phys. Rev. Appl. **9**, 064040 (2018).

[26] V. D. Tsiantos, T. Schrefl, W. Scholz, and J. Fidler, Thermal magnetization noise in submicrometer spin valve sensors, J. Appl. Phys. **93**, 8576 (2003).

[27] Y. G. Semenov, X. Xu, and K. W. Kim, Thermal fluctuations in antiferromagnetic nanostructures, arXiv:1806.11130v2.

[28] C. Lu, B. Gao, H. Wang, W. Wang, S. Yuan, S. Dong, and J.-M. Liu, Revealing controllable anisotropic magnetoresistance in spin-orbit coupled antiferromagnet Sr_2IrO_4, Adv. Funct. Mater. **28**, 1706589 (2018).